

Fourth-order quantum-chromodynamic corrections to the longitudinal coefficient function in deep-inelastic scattering

D. W. Duke, J. D. Kimel, and G. A. Sowell
 Florida State University, Tallahassee, Florida 32306
 (Received 13 August 1981)

We calculate the first non-leading-logarithmic corrections to the nonsinglet longitudinal structure function of deep-inelastic scattering, using the operator-product expansion and the renormalization group. We use dimensional regularization to regulate both ultraviolet and infrared divergences. We discuss the renormalization-scheme dependence of our result and its phenomenological implications.

I. INTRODUCTION

The longitudinal structure function is defined to be

$$F_L(x, Q^2) = \left[1 + \frac{4M^2 x^2}{Q^2} \right] F_2(x, Q^2) - 2xF_1(x, Q^2). \quad (1.1)$$

Neglecting $O(M^2/Q^2)$ effects, the naive parton-model result is just zero, as follows from the Callan-Gross relation.¹ The moments of F_L are given by

$$\langle F_L(Q^2) \rangle_n = C_{L,n}^{\text{NS}} \langle F_2(Q^2) \rangle_n + a C_{L,n}^{\text{S}} \langle xG(Q^2) \rangle_n,$$

where $a = \sum_q e_q^2$ for electroproduction, $G(Q^2)$ is the gluon distribution function, and x is the Bjorken scaling variable. The nonsinglet (NS) and singlet (S) coefficient functions are given to order g^2 by²⁻⁵

$$C_{L,n}^{\text{NS}} = \frac{\bar{g}^2}{16\pi^2} \frac{4C_F}{n+1}$$

and

$$C_{L,n}^{\text{S}} = \frac{\bar{g}^2}{16\pi^2} \frac{4T(R)}{(n+1)(n+2)}.$$

To compare this prediction with experiment, we look at the ratio of longitudinal- to transverse-photon cross sections. This is given by

$$R = \sigma_L / \sigma_T = \frac{F_L}{2xF_1}, \quad (1.2)$$

where σ_T and σ_L are the total cross sections for transverse and longitudinal virtual photons. Experimentally σ_T and σ_L can be extracted from the data using

$$\frac{d^2\sigma}{dQ^2 d\nu} = \Gamma(\sigma_T + \epsilon\sigma_L),$$

where ϵ is dependent on the beam energy and Γ is a flux factor. For several different ϵ 's a straight-line fit will yield σ_L as the slope and σ_T as the intercept. The measurement is difficult, however, since the cross section depends only weakly on R and is, therefore, susceptible to large systematic errors.

The first-order QCD prediction is consistent with the data⁶ for small x . For $x \gtrsim 0.3$ the prediction of the theory is systematically lower than the data^{4,7} even with its large error bars. The source of the disagreement may lie outside perturbative, twist-two QCD, being due, as some have suggested, to nucleon-mass effects, to the intrinsic transverse momenta of the constituent partons,⁸ to higher-twist effects,^{3,9} or to diquark systems in the nucleon.¹⁰ The source of the disagreement may also lie in large higher-order QCD corrections.

Indeed, it is clear by now that *no* meaningful comparison of a QCD-motivated scaling violation and experimental data is possible unless the theoretical prediction is extended beyond leading logarithms.¹¹ In this paper we calculate the first higher-order contribution to the Q^2 dependence of the moments of the nonsinglet longitudinal structure function $F_L(x, Q^2)$ of deep-inelastic scattering. These moments are inverted to give $F_L(x, Q^2)$ to order \bar{g}^4 . We then calculate R to this order.

Our procedure follows closely that of Ref. 12 except that we use on-shell, massless target quarks

instead of off-shell quarks. Both infrared and ultraviolet divergences are regulated by dimensional regularization. This has the advantage that all one-loop and many two-loop diagrams can be easily calculated analytically. In addition the handling of infrared divergences and their ultimate cancellation appear to us to be significantly simplified in this approach. This scheme has also been used in many perturbative cross-section calculations¹³⁻¹⁵ because of the simplicity of the massless phase-space integrations.

Our paper is organized as follows. In Sec. II we detail the formalism of this calculation and present the renormalization-group results. In Sec. III we give the order- g^2 results for the coefficient functions $C_{2,n}$ and $C_{L,n}$ as a demonstration of our method. The order- g^4 results and specific details of the calculation are discussed in Sec. IV. In Sec.

V we present the order- \bar{g}^4 nonsinglet correction to R and discuss its phenomenological implications. We briefly summarize our results in Sec. VI.

Finally, Appendix A contains our basic integrals and in Appendix B we collect the contributions from the individual Feynman diagrams for the order- g^4 calculation.

II. FORMALISM

A. Fundamentals

We consider the forward scattering of a photon current J_μ from a target of momentum p . The spin-averaged amplitude $T_{\mu\nu}$ for this process can be written as

$$\begin{aligned} T_{\mu\nu}(q,p) &= i \int d^4z e^{iq \cdot z} \langle p | T(J_\mu(z) J_\nu^\dagger(0)) | p \rangle_{\text{spin-averaged}} \\ &= e_{\mu\nu} T_L(q^2, \nu) + d_{\mu\nu} T_2(q^2, \nu), \end{aligned} \quad (2.1)$$

where q is the photon momentum and $\nu = p \cdot q$. The tensors $e_{\mu\nu}$ and $d_{\mu\nu}$ are given by

$$e_{\mu\nu} = g_{\mu\nu} - q_\mu q_\nu / q^2 \quad (2.2)$$

and

$$d_{\mu\nu} = -[g_{\mu\nu} - (p_\mu q_\nu + p_\nu q_\mu) / \nu + (p_\nu p_\nu / \nu^2) q^2]. \quad (2.3)$$

Specializing to nonsinglet amplitudes (e.g., $T_2^{ep} - T_2^{en}$), we expand the invariant amplitudes T_2 and T_L in inverse powers of x , the Bjorken variable ($-q^2/2\nu$). This gives

$$T_k = \sum_n \left[\frac{1}{x} \right]^n T_{k,n}, \quad k=2,L. \quad (2.4)$$

The $T_{k,n}$ are the moments of the deep-inelastic structure functions $F_2(x, Q^2)$ and $F_L(x, Q^2)$ (Ref. 16):

$$\begin{aligned} T_{k,n} &= M_{k,n} \\ &= \int dx x^{n-2} F_k(x, Q^2), \quad k=2,L, \end{aligned} \quad (2.5)$$

where $Q^2 = -q^2$. At this point we are neglecting target-mass corrections. These will be discussed in Sec. V.

On the other hand, applying the operator-product expansion for currents to Eq. (2.1) gives¹⁷

$$T_{k,n}(Q^2, \nu) = C_{k,n}(Q^2/\mu^2, g^2) A_n(\mu^2), \quad k=2,L, \quad (2.6)$$

where g^2 is the renormalized coupling constant, μ is the renormalization point, $C_{k,n}$ is the Q^2 -dependent coefficient function, and A_n is the reduced matrix element of the nonsinglet, twist-two operator,

$$\langle p | O_{\mu_1 \cdots \mu_n} | p \rangle = A_n p_{\mu_1} \cdots p_{\mu_n} + \text{traces},$$

where A_n does not depend on Q^2 . Thus, the Q^2 dependence of the moments $M_{k,n}$ is calculable when we know the coefficient function $C_{k,n}$. These are most easily determined by choosing quarks as target states. This means that $T_{k,n}$ and A_n are calculable in perturbation theory so that the $C_{k,n}$ are obtained order-by-order from Eq. (2.6).

Using Eqs. (2.1)–(2.4) and (2.6), we can project out the invariant amplitudes giving (in $4-2\epsilon$ dimensions)

$$T_{L,n} = \frac{4x^2}{Q^2} p^\mu p^\nu T_{\mu\nu}^{(n)} \quad (2.7)$$

and

$$T_{2,n} = \frac{1+\epsilon}{2} (-g^{\mu\nu} T_{\mu\nu}^{(n)}) + \frac{3+\epsilon}{2} T_{L,n}, \quad (2.8)$$

where

$$T_{\mu\nu} = \sum_n \left[\frac{1}{x} \right]^n T_{\mu\nu}^{(n)}.$$

Quark masses are set equal to zero.

B. Renormalization-group results

The Q^2 dependence of $C_{k,n}(Q^2/\mu^2, g^2)$ is determined by the renormalization-group equation

$$\left[\mu \frac{\partial}{\partial \mu} + \beta \frac{\partial}{\partial g} - \gamma_n \right] C_{k,n}(Q^2/\mu^2, g^2) = 0, \quad (2.9)$$

where $\gamma_n(g)$ is the anomalous dimension of the nonsinglet operator and $\beta(g)$ is defined by

$$\mu \frac{\partial g(\mu)}{\partial \mu} = \beta(g).$$

The solution of Eq. (2.9) is

$$\begin{aligned} C_{2,n}(Q^2/\mu^2, g^2) &= 1 + \frac{g^2}{16\pi^2} C_{2,n}^{(1)} + O(g^4) \\ &= 1 + \frac{g^2}{16\pi^2} \left[-\frac{\gamma_n^{(0)}}{2} \ln \frac{Q^2}{\mu^2} + B_{2,n}^{(1)} \right] + O(g^4) \end{aligned} \quad (2.12)$$

and

$$\begin{aligned} C_{L,n}(Q^2/\mu^2, g^2) &= \frac{g^2}{16\pi^2} C_{L,n}^{(1)} + \frac{g^4}{(16\pi^2)^2} C_{L,n}^{(2)} + O(g^6) \\ &= \frac{g^2}{16\pi^2} B_{L,n}^{(1)} + \frac{g^4}{(16\pi^2)^2} \left[\left[-\beta_0 - \frac{\gamma_n^{(0)}}{2} \right] B_{L,n}^{(1)} \ln \frac{Q^2}{\mu^2} + B_{L,n}^{(2)} \right] + O(g^6). \end{aligned} \quad (2.13)$$

Here we use the expansions

$$\begin{aligned} \beta(g) &= -\beta_0 \frac{g^3}{16\pi^2} - \beta_1 \frac{g^5}{(16\pi^2)^2} + O(g^7), \\ \gamma_n(g) &= \gamma_n^{(0)} \frac{g^2}{16\pi^2} + \gamma_n^{(1)} \frac{g^4}{(16\pi^2)^2} \\ &\quad + O(g^6), \end{aligned} \quad (2.14)$$

$$C_{2,n}(1, g^2) = 1 + \frac{g^2}{16\pi^2} B_{2,n}^{(1)} + O(g^4),$$

and

$$\begin{aligned} C_{L,n}(1, g^2) &= \frac{g^2}{16\pi^2} B_{L,n}^{(1)} + \frac{g^4}{(16\pi^2)^2} B_{L,n}^{(2)} \\ &\quad + O(g^6), \end{aligned} \quad (2.15)$$

where¹⁸

$$\beta_0 = \frac{11}{3} C_A - \frac{4}{3} T(R) \quad (2.16)$$

and

$$\begin{aligned} C_{k,n}(Q^2/\mu^2, g^2) &= C_{k,n}(1, \bar{g}^2) \\ &\quad \times \exp \left[- \int_{\bar{g}}^g d\bar{g}' \frac{\gamma_n(\bar{g}')}{\beta(\bar{g}')} \right], \end{aligned} \quad (2.10)$$

where \bar{g} is given by

$$\frac{d\bar{g}}{dt} = \beta(\bar{g}), \quad \bar{g}(t=0) = g, \quad (2.11)$$

with

$$t = \frac{1}{2} \ln \left[\frac{Q^2}{\mu^2} \right].$$

Expanding Eq. (2.10) in powers of g^2 gives

$$\gamma_n^{(0)} = 2C_F \left[1 - \frac{2}{n(n+1)} + 4 \sum_{j=2}^n \frac{1}{j} \right]. \quad (2.17)$$

The coefficients β_1 and $\gamma_n^{(1)}$ are given elsewhere.¹⁹ For a SU(N) gauge group we have $C_A = N$, $C_F = (N^2 - 1)/2N$, and $T(R) = \frac{1}{2}f$ for f flavors of quarks.

Finally, we define the expansions in g^2 of $T_{k,n}$ and A_n :

$$T_{2,n} = 1 + \frac{g^2}{16\pi^2} T_{2,n}^{(1)} + O(g^4), \quad (2.18)$$

$$\begin{aligned} T_{L,n} &= \frac{g^2}{16\pi^2} T_{L,n}^{(1)} + \frac{g^4}{(16\pi^2)^2} T_{L,n}^{(2)} \\ &\quad + O(g^6), \end{aligned} \quad (2.19)$$

and

$$A_n = 1 + \frac{g^2}{16\pi^2} A_n^{(1)} + O(g^4). \quad (2.20)$$

In Sec. III we review the calculation of $B_{2,n}^{(1)}$ and $B_{L,n}^{(1)}$. In Sec. IV we present an original calculation of $B_{L,n}^{(2)}$.

III. ORDER- g^2 RESULTS

The original calculation of $B_{2,n}^{(1)}$ used off-shell, massless quarks to regulate potential infrared divergences.¹² We use instead on-shell, massless quarks and let the infrared divergences be regulated by dimensional regularization.¹³

A. Calculation of $B_{L,n}^{(1)}$

Combining Eqs. (2.6), (2.7), (2.19), and (2.20), we have to order g^2

$$C_{L,n}^{(1)} = T_{L,n}^{(1)}.$$

The $p_\mu p_\nu$ projection in Eq. (2.7) means that only the Feynman diagram in Fig. 1(a) contributes to $T_{L,n}^{(1)}$. In this case there are no divergences and we get the well-known result⁵

$$T_{2,n}^{(1)} = C_F \left\{ \frac{1}{\epsilon_{UV}} + \frac{1}{\epsilon_{IR}} \left[-\frac{2}{n(n+1)} + 4S_n - 4 \right] + \left[\ln 4\pi - \gamma_E - \ln \frac{Q^2}{\mu^2} \right] \left[-\frac{2}{n(n+1)} + 4S_n - 3 \right] \right\} + B, \quad (3.4)$$

where

$$B = C_F \left[3S_n - 4 \sum_{j=1}^n \frac{1}{j^2} - \frac{2}{n(n+1)} S_n + 4 \sum_{j=1}^n \frac{1}{j} \sum_{k=1}^j \frac{1}{k} + \frac{3}{n} + \frac{4}{n+1} + \frac{2}{n^2} - 9 \right], \quad (3.5)$$

γ_E is Euler's constant, and $S_n = \sum_{j=1}^n 1/j$.

The diagrams of Fig. 2 contribute to $A_n^{(1)}$. Since we are using one-shell, massless-quark target states, each diagram is formally zero. This is due to the cancellation of an ultraviolet pole with an infrared pole.²⁰ In order to keep proper account of the different divergences we write the contributions of these diagrams as being proportional to

$$C_{L,n}^{(1)} = \frac{4C_F}{n+1}. \quad (3.1)$$

From Eq. (2.13) we see that

$$B_{L,n}^{(1)} = \frac{4C_F}{n+1}. \quad (3.2)$$

B. Calculation of $B_{2,n}^{(1)}$

Combining Eqs. (2.6), (2.8), (2.18), and (2.20), we have to order g^2

$$C_{2,n}^{(1)} = T_{2,n}^{(1)} - A_n^{(1)}. \quad (3.3)$$

The Feynman diagrams contributing to $T_{2,n}^{(1)}$ are shown in Fig. 1. These are calculable analytically in terms of gamma functions, beta functions, and hypergeometric functions. The relevant integrals are given in Appendix A. Diagrams with virtual corrections to the external quark legs will be discussed below. For clarity we distinguish the $1/\epsilon$ divergences due to the ultraviolet (UV) and infrared (IR) regions of the momentum integrations. Using Eq. (2.8) we get before renormalization

$$\frac{1}{\epsilon_{UV}} - \frac{1}{\epsilon_{IR}}.$$

The result for $A_n^{(1)}$ is, thus,

$$A_n^{(1)} = -C_F \left[-\frac{2}{n(n+1)} + 4S_n - 4 \right] \times \left[\frac{1}{\epsilon_{UV}} - \frac{1}{\epsilon_{IR}} \right]. \quad (3.6)$$

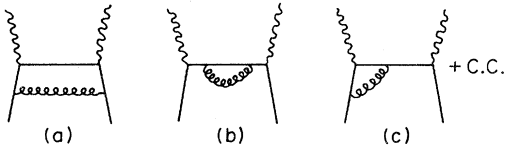


FIG. 1. Diagrams which contribute to $T_{L,n}^{(1)}$ and $T_{2,n}^{(1)}$. Crossed diagrams are assumed.



FIG. 2. Diagrams which contribute to $A_n^{(1)}$.

In contrast to the results of Ref. 12 there is no constant piece contributing to $A_n^{(1)}$ in our scheme.

After renormalization in the minimal-subtraction scheme we find from Eq. (3.3) that

$$C_{2,n}^{(1)} = -\frac{\gamma_n^{(0)}}{2} \ln \frac{Q^2}{\mu^2} + \frac{\gamma_n^{(0)}}{2} (\ln 4\pi - \gamma_E) + B,$$

with B given in Eq. (3.5). Comparing this with Eq. (2.12), we see that

$$B_{2,n}^{(1)} = \frac{\gamma_n^{(0)}}{2} (\ln 4\pi - \gamma_E) + B. \quad (3.7)$$

This result agrees with that of Ref. 12, but in our opinion the present calculation is considerably easier than the one presented there.

Diagrams with virtual corrections to the external quark legs for both $T_{2,n}^{(1)}$ and $A_n^{(1)}$ are also formally zero. The infrared divergences exactly cancel in the subtraction of Eq. (3.3) and, thus, these diagrams make no contribution to $B_{2,n}^{(1)}$. The same will also hold true for $B_{L,n}^{(2)}$.

IV. CALCULATION OF $B_{L,n}^{(2)}$

This calculation is the main object of our paper. Because of the $p_\mu p_\nu$ in Eq. (2.7), only the Feynman diagrams shown in Fig. 3 contribute to $T_{L,n}^{(2)}$. We

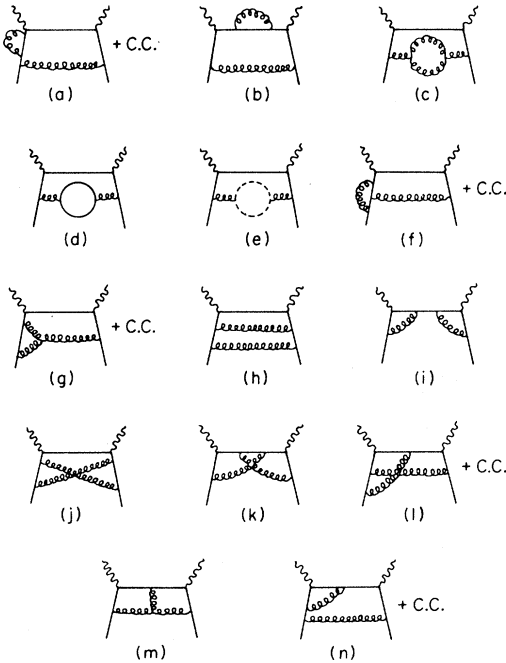


FIG. 3. Diagrams which contribute to $T_{L,n}^{(2)}$. Crossed diagrams are assumed.

have evaluated the diagrams of Figs. 3(a)–3(i) analytically and those of Figs. 3(j)–3(n) numerically. In the following subsections we discuss our methods for evaluating these diagrams and present the somewhat lengthy results in Appendix B.

A. Analytic calculation of $T_{L,n}^{(2)}$

The Feynman diagrams of Figs. 3(a)–3(i) were calculated analytically as products of hypergeometric functions, gamma functions, and beta functions. The relevant integrals are given in Appendix A. In this method it is easy to distinguish ultraviolet and infrared divergences since they appear as poles of gamma and beta functions, respectively. The algebraic tedium was alleviated to a large degree by extensive use of the algebraic-manipulation programs MACSYMA²¹ and GAMALG.²²

Not included in the diagrams of Fig. 3 are those with self-energy corrections to the external quark legs. As discussed above these make no net contribution to $B_{L,n}^{(2)}$. In addition the tadpole diagram is not shown since it is trivially zero.

The unrenormalized results for $T_{L,n}^{(2)}$ for the diagrams in Figs. 3(a)–3(i) are given in Appendix B 1. In Appendix B 2 the counterterms in the minimal-subtraction (MS) scheme for those diagrams with ultraviolet divergences are displayed. Included in Appendix B 2 is the counterterm for the diagram in Fig. 3(n). Even though we calculated this diagram numerically, we were able to extract the pole piece analytically.

B. Numerical calculation of $T_{L,n}^{(2)}$

For the Feynman diagrams of Figs. 3(j)–3(n) the propagator structures are sufficiently complicated that we were unable to calculate them analytically using the integrals of Appendix A. We explored several other means of analytically evaluating these diagrams, including the use of Gegenbauer polynomials.^{23,24} This latter method failed because it required either an integration over three Gegenbauer polynomials for Figs. 3(m) and 3(n), or an application to nonplanar diagrams [Figs. 3(j)–3(l)], both of which present formidable difficulties.

We did find, however, that by using the parametrization method of Ref. 25 we could write the integrands such that all momenta could be factored out leaving integrals of Feynman parameters only. Specifically, a typical integral has the form

$$I \propto \int dz_G \frac{A_1 + A_2 \omega}{(A_3 + A_4 \omega)^m},$$

$$I = \sum_n I_n \propto \sum_n \omega^n \int dz_G (A_5 + A_6 \omega),$$

where $\omega = 1/x$, the A_i are functions only of the Feynman parameters z_i , m is a function of the space-time dimension, and

$$dz_G = \prod_{i=1}^6 dz_i.$$

The integrands A_5 and A_6 are still sufficiently complicated so as to defy an exact evaluation. We chose, therefore, to use Monte Carlo integration.

To extract the divergences we evaluated the integral I_n in $4-2\epsilon$ dimensions. Specifically we calculated $I_n(\epsilon)$ for several values of ϵ and fitted the results to the polynomial

$$\epsilon I_n = P_n + F_n \epsilon + C_n \epsilon^2, \quad \epsilon \ll 1,$$

a form convenient for extracting the quantities of interest, P_n and F_n . A typical set of results is shown in Fig. 4. The technique proved sufficiently accurate that we were able to guess the *analytic* form of P_n as a function of the integer n for the diagrams in Figs. 3(j)–3(m). As mentioned above we were able to determine the pole structure of the diagram in Fig. 3(n) analytically. We then used these analytic pole pieces to give a better determination of F_n . In addition we have also checked several of the analytically evaluated diagrams using this method. The answers agreed to within the Monte Carlo integration errors, typically a few per cent.

The results of our numerical calculations are

$$\Sigma = C_F C_A \frac{44/3}{n+1} \left[\frac{1}{\epsilon_{UV}} + 2\psi \right] - C_F T(R) \frac{16/3}{n+1} \left[\frac{1}{\epsilon_{UV}} + 2\psi \right]$$

$$+ C_F^2 \left[\frac{4}{n+1} \left[-\frac{2}{n(n+1)} + 4S_n - 4 \right] \left[\frac{1}{\epsilon_{IR}} + 2\psi \right] + \frac{4}{n+1} \left[\frac{1}{\epsilon_{UV}} + 2\psi \right] \right] + \sum_i F_{i,n},$$

$$\psi = -\ln \left[\frac{Q^2}{\mu^2} \right] + \ln 4\pi - \gamma_E.$$

The $F_{i,n}$ are the finite pieces given in Appendices B 1 and B 3. The ultraviolet counterterms (MS scheme) are given in Appendix B 2 and sum to give

$$\Sigma' = C_F C_A \frac{44/3}{n+1} \left[\frac{1}{\epsilon_{UV}} + \psi \right] - C_F T(R) \frac{16/3}{n+1} \left[\frac{1}{\epsilon_{IR}} + \psi \right] + C_F^2 \frac{4}{n+1} \left[\frac{1}{\epsilon_{UV}} + \psi \right] + \sum_i F'_{i,n},$$

where the $F'_{i,n}$ are also given in Appendix B 2. The renormalized $T_{L,n}^{(2)}$ is, thus,

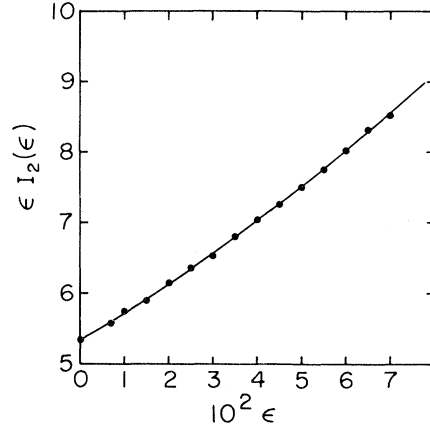


FIG. 4. Typical numerical evaluation of a diagram, showing a linear fit to the Monte Carlo integration “data” points. The error bars are too small to be seen on this scale. This figure corresponds to the $n=2$ moment of the diagram in Fig. 3(n).

given in Appendix B 3. We have evaluated the first five even moments for each of these diagrams for $f=4$ flavors. The errors shown result from the uncertainties of Monte Carlo integration.

C. Results for $B_{L,n}^{(2)}$

At order g^4 we have from Eqs. (2.6), (2.19), and (2.20)

$$C_{L,n}^{(2)} = T_{L,n}^{(2)} - C_{L,n}^{(1)} A_n^{(1)}. \quad (4.1)$$

The sum of all the diagrams in Fig. 3 yields for $T_{L,n}^{(2)}$, before renormalization,

$$\begin{aligned}
T_{L,n}^{(2)} &= \Sigma - \Sigma' \\
&= \frac{4C_F}{n+1} \left[\beta_0 + \frac{\gamma_n^{(0)}}{2} \right] \psi + \frac{4C_F^2}{n+1} \left[-\frac{2}{n(n+1)} + 4S_n - 4 \right] \left[\frac{1}{\epsilon_{\text{IR}}} + \psi \right] + \sum_i (F_{i,n} - F'_{i,n}). \quad (4.2)
\end{aligned}$$

For the second term of Eq. (4.1) the result of Eq. (3.1) for $C_{L,n}^{(1)}$ is not sufficient. Because of the infrared pole in $A_n^{(1)}$ [Eq. (3.6)], we must keep the $O(\epsilon)$ piece of $C_{L,n}^{(1)}$. The product $C_{L,n}^{(1)}A_n^{(1)}$ is given after renormalization ($\overline{\text{MS}}$ scheme) by

$$C_{L,n}^{(1)}A_n^{(1)} = \frac{4C_F^2}{n+1} \left[-\frac{2}{n(n+1)} - 4S_n - 4 \right] \left[\frac{1}{\epsilon_{\text{IR}}} + \psi \right] + F_{\text{IR},n},$$

where

$$F_{\text{IR},n} = \frac{4C_F^2}{n+1} \left[-\frac{2}{n(n+1)} + 4S_n - 4 \right] (S_n + 1). \quad (4.3)$$

The final answer for $C_{L,n}^{(2)}$ is

$$C_{L,n}^{(2)} = \sum_i (F_{i,n} - F'_{i,n}) - F_{\text{IR},n} + \frac{4C_F}{n+1} \left[-\beta_0 - \frac{\gamma_n^{(0)}}{2} \right] \left[\ln \frac{Q^2}{\mu^2} - \ln 4\pi + \gamma_E \right]. \quad (4.4)$$

Comparing this with Eq. (2.13), we see that the coefficient of the $\ln(Q^2/\mu^2)$ is as expected from the renormalization-group equation and that

$$B_{L,n}^{(2)} = \sum_i (F_{i,n} - F'_{i,n}) - F_{\text{IR},n} + \frac{4C_F}{n+1} \left[\beta_0 + \frac{\gamma_n^{(0)}}{2} \right] (\ln 4\pi - \gamma_E). \quad (4.5)$$

In the $\overline{\text{MS}}$ scheme of Ref. 12 the final term containing $(\ln 4\pi - \gamma_E)$ is absent.

Using Eq. (2.15) we can write

$$C_{L,n}(1, \bar{g}^2) = \frac{\bar{g}^2}{16\pi^2} B_{L,n}^{(1)} \left[1 + \frac{\bar{g}^2}{16\pi^2} R_{L,n}^{(2)} \right],$$

where

$$R_{L,n}^{(2)} = B_{L,n}^{(2)} / B_{L,n}^{(1)}.$$

The numerical results for $R_{L,n}^{(2)}$ in the $\overline{\text{MS}}$ scheme and the momentum-subtraction (MOM) scheme are given in Table I. Here we have used $f=4$ for the number of flavors. The errors shown are Monte Carlo integration errors.

We summarize the renormalization-scheme dependence of our results by relating the MS and MOM schemes to the $\overline{\text{MS}}$ scheme. In the MS scheme²⁶

$$\begin{aligned}
\Lambda_{\text{MS}} &= \exp\left[-\frac{1}{2}(\ln 4\pi - \gamma_E)\right] \Lambda_{\overline{\text{MS}}} \\
&= \frac{1}{2.65} \Lambda_{\overline{\text{MS}}}
\end{aligned}$$

and

$$R_{L,n,\text{MS}}^{(2)} = R_{L,n,\overline{\text{MS}}}^{(2)} + \left[\beta_0 + \frac{\gamma_n^{(0)}}{2} \right] (\ln 4\pi - \gamma_E).$$

In the momentum-subtraction scheme²⁴

TABLE I. Numerical results for $R_{L,n}^{(2)}$ for $n=2, 4, 6, 8, 10$ in the $\overline{\text{MS}}$ and MOM renormalization schemes corresponding to $f=4$ flavors.

n	$R_{L,n,\overline{\text{MS}}}^{(2)}$	$R_{L,n,\text{MOM}}^{(2)}$
2	17.6±0.6	-0.8±0.6
4	31.0±0.8	7.3±0.8
6	37.9±0.7	11.0±0.7
8	43.9±0.8	14.8±0.8
10	49.4±1.0	18.5±1.0

$$\begin{aligned}\Lambda_{\text{MOM}} &= \exp\left[\frac{1}{2}(1.55)\right]\Lambda_{\overline{\text{MS}}} \\ &= 2.17\Lambda_{\overline{\text{MS}}}\end{aligned}$$

and

$$R_{L,n,\text{MOM}}^{(2)} = R_{L,n,\overline{\text{MS}}}^{(2)} - \left[\beta_0 + \frac{\gamma_n^{(0)}}{2} \right] \quad (1.55)$$

V. PHENOMENOLOGY

In this section we describe the procedure used to determine (approximately) $F_2(x, Q^2)$ and $F_L(x, Q^2)$ using the moments we have calculated. Combining Eqs. (2.5), (2.6), (2.10), and the expansions of $\beta(\bar{g})$, $\gamma_n(\bar{g})$, and $C_{k,n}(1, \bar{g}^2)$, we find

$$M_{2,n}(Q^2) = A_n \left[\frac{\bar{g}^2}{16\pi^2} \right]^{d_n} \left[1 + \frac{\bar{g}^2}{16\pi^2} \left[B_{2,n}^{(1)} + \frac{\gamma_n^{(1)}}{2\beta_0} - \frac{\beta_1 \gamma_n^{(0)}}{2\beta_0^2} \right] \right] \quad (5.1)$$

and

$$M_{L,n}(Q^2) = A_n \left[\frac{\bar{g}^2}{16\pi^2} \right]^{d_n+1} \frac{4C_F}{n+1} \left[1 + \frac{\bar{g}^2}{16\pi^2} \left[R_{L,n}^{(2)} + \frac{\gamma_n^{(1)}}{2\beta_0} - \frac{\beta_1 \gamma_n^{(0)}}{2\beta_0^2} \right] \right], \quad (5.2)$$

where $d_n = \gamma_n^{(0)}/2\beta_0$.

In terms of experimentally measured distributions $F_2(x, Q^2)$ and $F_L(x, Q^2)$, these moments are given by the Nachtmann formulas

$$\int_0^1 dx \frac{\xi^{n+1}}{x^3} \left[\frac{3+3(n+1)r+n(n+2)r^2}{(n+2)(n+3)} \right] F_2(x, Q^2) = M_{2,n}(Q^2) \quad (5.3)$$

and

$$\int_0^1 dx \frac{\xi^{n+1}}{x^3} \left[\frac{2}{3} r^2 F_2(x, Q^2) - F_L(x, Q^2) \right] = \frac{2}{3} M_{2,n}(Q^2) - M_{L,n}(Q^2), \quad (5.4)$$

where $\xi = 2x/(1+r)$ and $r = (1+4M^2x^2/Q^2)^{1/2}$. Setting $M^2=0$ we regain Eq. (2.5). We will show results corresponding to both $M^2=0$ and $M^2=0.88 \text{ GeV}^2$.

Given a function $F_2(x, Q_0^2)$ at some Q_0^2 as input, we may easily use Eqs. (5.1) and (5.3) to determine the constants A_n . For the purposes of this paper we have chosen simply

$$F_2(x, Q_0^2) = 5 \text{ GeV}^2 = 2x^{1/2}(1-x)^3.$$

This function has roughly the shape expected for a nonsinglet quark distribution in a nucleon. Note that the overall normalization will not contribute to $R = \sigma_L/\sigma_T$.

To invert the moments in Eq. (5.1), we follow the method of Ref. 27. The inversion follows a simple two-step procedure. First we make the provisional assumption that the structure function $F_2(x, Q^2)$ has the form

$$F_2(x, Q^2) = Ax^\alpha(1-x)^\beta.$$

We fit the moments [Eq. (5.3)] of this equation for $2 \leq n \leq n_{\text{max}}$ to the results of Eq. (5.1) to determine α and β . We next assume a parametrization for $F_2(x, Q^2)$ of the form

$$F_2(x, Q^2) = x^\alpha(1-x)^\beta \sum_{m=0}^M a_m x^m, \quad (5.5)$$

where $M \leq n_{\text{max}} - 2$ with α and β as determined above. A fit of the moments of this equation to the results of Eq. (5.1) now involves only a simple linear least-squares fit to determine the a_m 's. Generally $M \sim 3-5$ will give sufficiently accurate results. For our calculation $n_{\text{max}} = 10$ and $M = 3$.

We now repeat this procedure for $F_L(x, Q^2)$ using Eqs. (5.2), (5.4), and the $F_2(x, Q^2)$ just determined.

Before we can invert the moments, one further point must be specified. We need the odd as well as the even moments to carry out the inversion. The odd moments were eliminated in the calculations of Secs. III and IV when we added a diagram with its crossed version. This sum has the general form

$$B_n + (-1)^n B_n.$$

In practice we calculate a diagram, multiply by two, and restrict the expansion in $\omega = 1/x$ to even powers. To analytically continue the results to odd moments we assume they have the following form for *odd* n (Ref. 28):

$$B_n - (-1)^n B_n .$$

We now calculate a diagram and multiply by two for *all* n .

This procedure is straightforward for the planar diagrams of Figs. 1 and 3. For the nonplanar diagrams of Figs. 3(j) and 3(l) the situation is more complicated. Factors of $(-1)^n$ are present in the results of these diagrams as well as between the sum of a diagram and its crossed version. We did not isolate these factors in our numerical integrations, but chose instead to interpolate by smooth curves the values of the odd moments from the even moments. We also applied this method to the other diagrams we calculated numerically, Figs. 3(k), 3(m), and 3(n). Since these diagrams have only a small effect on the total results, we feel justified in using our approximate interpolation.

Using the method just described we have approximately reconstructed $F_2(x, Q^2)$ and $F_L(x, Q^2)$ in leading and next-to-leading orders both with and without target-mass corrections. For the leading-order (LO) reconstruction the running coupling constant \bar{g} is specified by

$$\frac{\bar{g}_{LO}^2}{16\pi^2} = \frac{1}{\beta_0 \ln(Q^2/\Lambda_{LO}^2)} .$$

For the higher-order (HO) calculation \bar{g} is obtained by solving numerically

$$\frac{16\pi^2}{\beta_0 \bar{g}_{HO}^2} - \frac{\beta_1}{\beta_0^2} \ln \left[\frac{16\pi^2}{\beta_0 \bar{g}_{HO}^2} + \frac{\beta_1}{\beta_0^2} \right] = \ln \frac{Q^2}{\Lambda_{\overline{MS}}^2} .$$

For the case of no target-mass corrections ($M^2=0$) we used $\Lambda_{LO}=650$ MeV and $\Lambda_{\overline{MS}}=500$ MeV. For a target mass of $M^2=0.88$ GeV² we chose $\Lambda_{LO}=550$ MeV and $\Lambda_{\overline{MS}}=450$ MeV. These values of Λ were selected so that the predicted evolution with Q^2 of $F_2(x, Q^2)$ was approximately the same in the four cases.

As an example of the effects of our choices for the Λ 's on \bar{g} , we get for $Q^2=5$ GeV² the values $\bar{g}_{LO}^2/16\pi^2=0.049$ and $\bar{g}_{HO}^2/16\pi^2=0.029$ for the case of $M^2=0$. The combined effect of this decrease in the size of the coupling constant and the positive contributions from the higher-order corrections (see Table I) means that, in fact, the leading-order and next-to-leading-order predictions for $R = \sigma_L/\sigma_T$ are essentially the same (to within a few percent). This is not to say that the order- \bar{g}^4 corrections to F_L are insignificant. Indeed, as indicated by the numbers in Table I they are large. This result is more a reflection of our requiring $F_2(x, Q^2)$ to have approximately the same form for

both leading and next-to-leading order, which determines our choices of Λ . Including the target-mass corrections also produces similar results for the two orders.

In Fig. 5 we present our theoretical predictions for R . Curve (a) has no target-mass corrections, while curve (b) includes them. As mentioned, the leading and next-to-leading-order results are essentially the same for both cases. The data are from SLAC²⁹ and are shown for comparison.

VI. SUMMARY

In this paper we have presented a calculation for the nonsinglet, longitudinal, Wilson coefficient function $C_{L,n}(Q^2/\mu^2, g^2)$ to order g^4 . The use of massless, on-shell target quarks and of dimensional regularization for isolating both the ultraviolet and infrared singularities enabled us to do all one-loop and many two-loop diagrams analytically. The handling of infrared singularities was particularly simplified in this approach in comparison to the method of using off-shell quarks for regularization.

For those diagrams which could not be done analytically numerical techniques were employed.

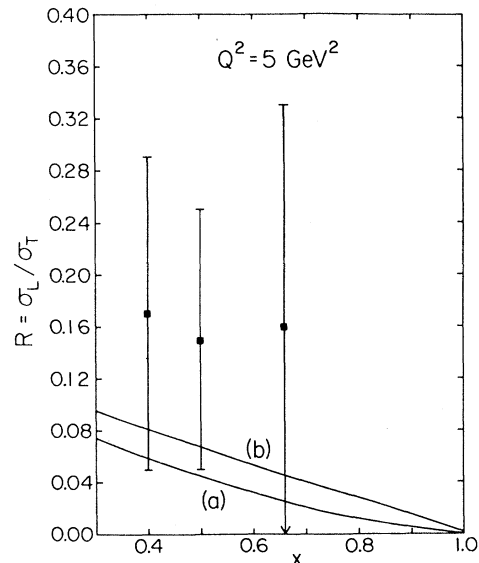


FIG. 5. Theoretical predictions for R . (a) No target-mass corrections with $\Lambda_{LO}=650$ MeV or $\Lambda_{\overline{MS}}=500$ MeV. (b) Including target-mass corrections with $\Lambda_{LO}=550$ or $\Lambda_{\overline{MS}}=450$ MeV. As discussed in the text, when all the higher-order corrections are included, there is essentially no change with respect to the leading-order prediction. The data are from SLAC (Ref. 29).

In the course of the numerical part of the calculation we used a general fitting procedure for determining the ϵ dependence of the Compton amplitudes. This technique proved sufficiently accurate that we were able to surmise the analytic form of the $1/\epsilon$ terms. This, in turn, was useful in allowing us to compare the Q^2 dependence of our results with the renormalization-group prediction.

The order- g^4 corrections to the coefficient function were large as indicated in Table I. We found that the non-Abelian graphs of Fig. 3 dominate the results by virtue of their larger color factors. In addition the importance of the uncertainties due to the Monte Carlo integrations required for the diagrams calculated numerically is reduced since the contributions of these diagrams are small in comparison to those calculated analytically.

Finally, in Sec. V we calculated $R = \sigma_L/\sigma_T$ to order \bar{g}^4 . This involved using our results for

$$I_{a,b;N}(p) = \int \frac{d^n k}{(2\pi)^n} \frac{k_{\mu_1} \cdots k_{\mu_N}}{k^{2a}(k+p)^{2b}}$$

$$= \frac{i(-1)^{N+n/2}}{(4\pi)^{n/2}} \frac{\Gamma(a+b-n/2)}{\Gamma(a)\Gamma(b)} B \left[\frac{n}{2} - b, \frac{n}{2} - a + N \right] (p^2)^{n/2-(a+b)} p_{\mu_1} \cdots p_{\mu_N} + I',$$

where $p^2 \neq 0$. Those terms proportional to $g_{\mu\nu}$ were not needed in our calculation and are collected in the quantity I' ,

$$K_{a,b,c;N}(p,q) = \int \frac{d^n k}{(2\pi)^n} \frac{k_{\mu_1} \cdots k_{\mu_N}}{k^{2a}(k+p)^{2b}(k+q)^{2c}}$$

$$= \frac{i(-1)^{N+n/2}}{(4\pi)^{n/2}} \frac{\Gamma(a+b+c-n/2)}{\Gamma(a)\Gamma(b)\Gamma(c)} B \left[\frac{n}{2} - c, \frac{n}{2} - (a+b) + N \right]$$

$$\times B(a,b)_2 F_1 \left[a+b+c - \frac{n}{2}, b; a+b; \alpha \right] (q^2)^{n/2-(a+b+c)} q_{\mu_1} \cdots q_{\mu_N} + K',$$

where $p^2=0$, $q^2 \neq 0$, and

$$\alpha = \frac{2p \cdot q}{q^2}.$$

Those terms proportional to $g_{\mu\nu}$ and p_μ were not needed in our calculation and are collected in the quantity K' .

APPENDIX B: RESULTS FOR THE FEYNMAN DIAGRAMS OF FIG. 3

The Feynman diagrams of Fig. 3 are referenced by their figure numbers.

$C_{L,n}(Q^2/\mu^2, g^2)$ and the moment-inversion technique of Ref. 27. We found that R is essentially insensitive to the higher-order corrections because of the significant cancellations of these corrections in the numerator and denominator of the ratio σ_L/σ_T .

ACKNOWLEDGMENTS

We thank the MATHLAB at MIT for the use of MACSYMA. This research was supported in part by the U.S. Department of Energy.

APPENDIX A: BASIC INTEGRALS

The following integrals are used in calculating the analytic results of this paper:

1. Unrenormalized contributions to $T_{L,n}^{(2)}$: Analytic results

The contribution of Fig. 3(a) is given by

$$C_F^2 \left[-\frac{8}{n+1} \left[\frac{1}{\epsilon_{UV}} + 2\psi \right] \right] + F_{a,n},$$

where $\psi = -\ln(Q^2/\mu^2) + \ln 4\pi - \gamma_E$, and

$$F_{a,n} = C_F^2 \left[-\frac{8}{n+1} \left[S_n - \frac{1}{n+1} + \frac{7}{2} \right] \right].$$

The contribution of Fig. 3(b) is given by

$$C_F^2 \left[-\frac{4}{n+1} \left[\frac{1}{\epsilon_{UV}} + 2\psi \right] \right] + F_{b,n},$$

where

$$F_{b,n} = C_F^2 \left[-\frac{4}{n+1} \left[2S_n + \frac{5}{2} \right] \right].$$

The contribution of Fig. 3(c) includes the combinatoric factor of $\frac{1}{2}$ and is given by

$$C_F C_A \left[\frac{19/3}{n+1} \left[\frac{1}{\epsilon_{UV}} + 2\psi \right] \right] + F_{c,n},$$

where

$$F_{c,n} = C_F C_A \left[\frac{19/3}{n+1} \left[2S_n - \frac{1}{n} - \frac{1}{n+1} + \frac{517}{114} \right] \right].$$

The contribution of Fig. 3(d) is given by

$$C_F T(R) \left[-\frac{16/3}{n+1} \left[\frac{1}{\epsilon_{UV}} + 2\psi \right] \right] + F_{d,n},$$

where

$$F_{d,n} = (C_F^2 - C_F C_A / 2) \left\{ -\frac{8}{n+1} \left[\left[1 - \frac{2}{n} \right] \left[2S_n - \frac{1}{n} - \frac{1}{n+1} \right] - S_n - \frac{7}{n} + \frac{13}{2} \right] \right\}.$$

The contribution of Fig. 3(g) is given by

$$C_F C_A \left[\frac{8(S_n - 1)}{n+1} \left[\frac{1}{\epsilon_{IR}} + 2\psi \right] + \frac{12}{n+1} \left[\frac{1}{\epsilon_{UV}} + 2\psi \right] \right] + F_{g,n},$$

where

$$F_{g,n} = C_F C_A \left[\frac{4}{n+1} (1 + 2S_n) \left[S_n - \frac{1}{n+1} + \frac{5}{2} \right] + 2 \sum_{k=1}^n \frac{1}{k} S_{k-1} + \left[S_n + \frac{1}{n} + 2 \right] \right].$$

The contribution of Fig. 3(h) is given by

$$C_F^2 \left[-\frac{8}{n(n+1)^2} \left[\frac{1}{\epsilon_{IR}} + 2\psi \right] \right] + F_{h,n},$$

where

$$F_{h,n} = C_F^2 \left[-\frac{8}{n(n+1)^2} \left[2S_n - \frac{1}{n} - \frac{1}{n+1} + \frac{3}{2} \right] \right].$$

The contribution of Fig. 3(i) is given by

$$F_{i,n},$$

where

$$F_{i,n} = C_F^2 \sum_{k=1}^n \frac{-4}{k(n-k+1)}.$$

$$F_{d,n} = C_F T(R) \left[-\frac{16/3}{n+1} \left[2S_n - \frac{1}{n} - \frac{1}{n+1} + \frac{25}{6} \right] \right].$$

The contribution of Fig. 3(e) is given by

$$C_F C_A \left[\frac{1/3}{n+1} \left[\frac{1}{\epsilon_{UV}} + 2\psi \right] \right] + F_{e,n},$$

where

$$F_{e,n} = C_F C_A \left[\frac{1/3}{n+1} \left[2S_n - \frac{1}{n} - \frac{1}{n+1} + \frac{31}{6} \right] \right].$$

The contribution of Fig. 3(f) is given by

$$(C_F^2 - C_F C_A / 2) \left[-\frac{8(2-2/n)}{n+1} \left[\frac{1}{\epsilon_{IR}} + 2\psi \right] + \frac{8}{n+1} \left[\frac{1}{\epsilon_{UV}} + 2\psi \right] \right] + F_{f,n},$$

where

2. Counterterm contributions to $T_{L,n}^{(2)}$

The contribution of Fig. 3(a) is given by

$$C_F^2 \left[-\frac{8}{n+1} \left[\frac{1}{\epsilon_{UV}} + \psi \right] \right] + F'_{a,n},$$

where

$$F'_{a,n} = C_F^2 \left[-\frac{8}{n+1} (1 + S_n) \right].$$

The contribution of Fig. 3(b) is given by

$$C_F^2 \left[-\frac{4}{n+1} \left[\frac{1}{\epsilon_{UV}} + \psi \right] \right] + F'_{b,n},$$

where

TABLE II. The values $F_{i,n}$ for those diagrams calculated numerically [Figs. 3(j)–3(n)].

n	$F_{j,n}$	$F_{k,n}$	$F_{l,n}$	$F_{m,n}$	$F_{n,n}$
2	0.7 ± 0.1	-0.7 ± 0.1	-7.9 ± 0.2	-16.1 ± 0.2	17.7 ± 1.0
4	0.7 ± 0.1	-0.5 ± 0.1	-8.0 ± 0.2	-9.4 ± 0.3	13.1 ± 0.7
6	0.5 ± 0.1	-0.4 ± 0.1	-7.3 ± 0.1	-6.4 ± 0.3	8.5 ± 0.4
8	0.4 ± 0.1	-0.4 ± 0.1	-6.9 ± 0.1	-5.0 ± 0.3	6.8 ± 0.4
10	0.2 ± 0.1	-0.3 ± 0.1	-6.2 ± 0.1	-4.3 ± 0.3	5.9 ± 0.4

$$F'_{b,n} = C_F^2 \left[-\frac{4}{n+1} (1+S_n) \right].$$

The contribution of Fig. 3(c) including the combinatoric factor of $\frac{1}{2}$ is given by

$$C_F C_A \left[\frac{19/3}{n+1} \left[\frac{1}{\epsilon_{UV}} + \psi \right] \right] + F'_{c,n},$$

where

$$F'_{c,n} = C_F C_A \left[\frac{19/3}{n+1} (1+S_n) \right].$$

The contribution of Fig. 3(d) is given by

$$C_F T(R) \left[-\frac{16/3}{n+1} \left[\frac{1}{\epsilon_{UV}} + \psi \right] \right] + F'_{d,n},$$

where

$$F'_{d,n} = C_F T(R) \left[-\frac{16/3}{n+1} (1+S_n) \right].$$

The contribution of Fig. 3(e) is given by

$$C_F C_A \left[\frac{1/3}{n+1} \left[\frac{1}{\epsilon_{UV}} + \psi \right] \right] + F'_{e,n},$$

where

$$F'_{e,n} = C_F C_A \left[\frac{1/3}{n+1} (1+S_n) \right].$$

The contribution of Fig. 3(f) is given by

$$(C_F^2 - C_F C_A / 2) \left[\frac{8}{n+1} \left[\frac{1}{\epsilon_{UV}} + \psi \right] \right] + F'_{f,n},$$

where

$$F'_{f,n} = (C_F^2 - C_F C_A / 2) \left[\frac{8}{n+1} (1+S_n) \right].$$

The contribution of Fig. 3(g) is given by

$$C_F C_A \left[\frac{12}{n+1} \left[\frac{1}{\epsilon_{UV}} + \psi \right] \right] + F'_{g,n},$$

where

$$F'_{g,n} = C_F C_A \left[\frac{12}{n+1} (1+S_n) \right].$$

The contribution of Fig. 3(n) is given by

$$C_F^2 \left[\frac{8}{n+1} \left[\frac{1}{\epsilon_{UV}} + \psi \right] \right] + F'_{n,n},$$

where

$$F'_{n,n} = C_F^2 \left[\frac{8}{n+1} (1+S_n) \right].$$

3. Contributions to $T_{L,n}^{(2)}$: Numerical results

The contribution of Fig. 3(j) is given by

$$(C_F^2 - C_F C_A / 2) \left[-\frac{16}{n(n+1)} \left[\frac{1}{\epsilon_{IR}} + 2\psi \right] \right] + F_{j,n},$$

where $F_{j,n}$ is given in Table II for $n=2, 4, 6, 8, 10$. The contribution of Fig. 3(k) is given by

$$F_{k,n},$$

where $F_{k,n}$ is given in Table II for $n=2, 4, 6, 8, 10$. The contribution of Fig. 3(l) is given by

$$(C_F^2 - C_F C_A / 2) \left[\frac{16S_n}{n+1} \left[\frac{1}{\epsilon_{IR}} + 2\psi \right] \right] + F_{l,n},$$

where $F_{l,n}$ is given in Table II for $n=2, 4, 6, 8, 10$. The contribution of Fig. 3(m) is given by

$$F_{m,n},$$

where $F_{m,n}$ is given in Table II for $n=2, 4, 6, 8, 10$. The contribution of Fig. 3(n) is given by

$$C_F^2 \left[\frac{8}{n+1} \left[\frac{1}{\epsilon_{UV}} + 2\psi \right] \right] + F_{n,n},$$

where $F_{n,n}$ is given in Table II for $n=2, 4, 6, 8, 10$.

- ¹C. G. Callan and D. J. Gross, Phys. Rev. Lett. 22, 156 (1969).
- ²M. Calvo, Phys. Rev. D 15, 730 (1977).
- ³D. Nanopoulos and G. Ross, Phys. Lett. 58B, 105 (1975).
- ⁴I. Hinchliffe and C. H. Llewellyn Smith, Nucl. Phys. B128, 93 (1977).
- ⁵A. Zee, F. Wilczek, and S. B. Treiman, Phys. Rev. D 10, 2881 (1974).
- ⁶B. A. Gordon *et al.*, Phys. Rev. D 20, 2645 (1979).
- ⁷A. De Rújula, H. Georgi, and H. D. Politzer, Ann. Phys. (N.Y.) 103, 315 (1977).
- ⁸M. Glück and E. Reya, Nucl. Phys. B145, 24 (1978).
- ⁹L. F. Abbott, W. B. Atwood, and R. M. Barnett, Phys. Rev. D 22, 582 (1980).
- ¹⁰I. A. Schmidt and R. Blankenbecler, Phys. Rev. D 16, 1318 (1977); L. F. Abbott, E. L. Berger, R. Blankenbecler, and G. Kane, Phys. Lett. 88B, 157 (1978).
- ¹¹A. J. Buras, Rev. Mod. Phys. 52, 199 (1980).
- ¹²W. A. Bardeen, A. J. Buras, D. W. Duke, and T. Muta, Phys. Rev. D 18, 3998 (1978).
- ¹³G. Altarelli, R. K. Ellis, and C. Martinelli, Nucl. Phys. B143, 521 (1978); B146, 544(E); B157, 461 (1979).
- ¹⁴G. Altarelli, R. K. Ellis, C. Martinelli, and S. Y. Pi, Nucl. Phys. B160, 301 (1979).
- ¹⁵R. K. Ellis, M. A. Furman, H. E. Haber, and I. Hinchliffe, Nucl. Phys. B173, 397 (1980); R. K. Ellis, D. A. Ross, and A. E. Terrano, Phys. Rev. Lett. 45, 1226 (1980); Nucl. Phys. B178, 421 (1981).
- ¹⁶N. Christ, B. Hasslacher, and A. Mueller, Phys. Rev. D 6, 3543 (1972).
- ¹⁷K. Wilson, Phys. Rev. 179, 1499 (1969).
- ¹⁸H. D. Politzer, Phys. Rev. Lett. 30, 1346 (1973); H. Georgi and H. D. Politzer, Phys. Rev. D 9, 416 (1974); D. J. Gross and F. Wilczek, Phys. Rev. Lett. 30, 1323 (1973); Phys. Rev. D 8 3633 (1973); 9, 980 (1974).
- ¹⁹D. R. T. Jones, Nucl. Phys. B75, 531 (1974); W. Caswell, Phys. Rev. Lett. 33, 244 (1974); E. G. Floratos, D. A. Ross, and C. T. Sachrajda, Nucl. Phys. B129, 66 (1977); B139, 545 (E).
- ²⁰W. A. Bardeen, B. W. Lee, and R. E. Shrock, Phys. Rev. D 14, 985 (1976); P. Cvitanović, Nucl. Phys. B130, 114 (1977).
- ²¹MATHLAB Group, MIT Laboratory for Computer Science, MACSYMA Reference Manual, Version 9, (unpublished).
- ²²S. Wolfram, Caltech Report No. CALT-68-736, 1979 (unpublished).
- ²³A. Terrano, Phys. Lett. 933, 424 (1980).
- ²⁴W. Celmaster and R. J. Gonsalves, Phys. Rev. D 21, 3112 (1980).
- ²⁵P. Cvitanović and T. Kinoshita, Phys. Rev. D 10, 3978 (1974).
- ²⁶G. 't Hooft, Nucl. Phys. B61, 455 (1973); G. 't Hooft and M. Veltman, *ibid.* 44, 189 (1972).
- ²⁷D. W. Duke and R. G. Roberts, Nucl. Phys. B166, 243 (1980).
- ²⁸D. A. Ross and C. T. Sachrajda, Nucl. Phys. B149, 497 (1979).
- ²⁹M. D. Mestayer, SLAC Report No. 214, 1974 (unpublished).